Influence of the structure on the properties of red phosphors

Influence of the Structure on the Properties of $Na_xEu_y(MoO_4)_z$ Red Phosphors

Vladimir A. Morozov, Bogdan I. Lazoryak, Semen Z. Shmurak, Aleksander P. Kiselev, Oleg I. Lebedev, Nicolas Gauquelin, Johan Verbeeck, Joke Hadermann, and Gustaaf Van Tendeloo

Chemistry of Materials, 26, 3238 - 3248, (2014)

Influence of the Structure on the Properties of $Na_xEu_y(MoO_4)_z$ Red Phosphors

Vladimir A. Morozov,[†,∥] Bogdan I. Lazoryak,[†] Semen Z. Shmurak,[‡] Aleksander P. Kiselev,[‡] Oleg I. Lebedev,[§] Nicolas Gauquelin,[∥] Johan Verbeeck,[∥] Joke Hadermann,*[,∥] and Gustaaf Van Tendeloo[∥]

ABSTRACT: Scheelite related compounds $(A',A'')_n[(B',B'')O_4]_m$ with B′, B″ = W and/or Mo are promising new materials for red phosphors in pc-WLEDs (phosphor-converted white-light-emitting-diode) and solid-state lasers. Cation substitution in $CaMoO_4$ of Ca^{2+} by the combination of Na^+ and Eu^{3+}, with the creation of A cation vacancies, has been investigated as a factor for controlling the scheelite-type structure and the luminescent properties. $Na_5Eu(MoO_4)_4$ and $Na_xEu^{3+}{}_{(2-x)/3}\square_{(1-2x)/3}MoO_4$ ($0.138 \leq x \leq 0.5$) phases with a scheelite-type structure were synthesized by the solid state method; their structural characteristics were investigated using transmission electron microscopy. Contrary to powder synchrotron X-ray diffraction before, the study by electron diffraction and high resolution transmission electron microscopy in this paper revealed that $Na_{0.286}Eu_{0.571}MoO_4$ has a (3 + 2)D incommensurately modulated structure and that (3 + 2)D incommensurately modulated domains are present in $Na_{0.200}Eu_{0.600}MoO_4$. It also confirmed the (3 + 1)D incommensurately modulated character of $Na_{0.138}Eu_{0.621}MoO_4$. The luminescent properties of all phases under near-ultraviolet (n-UV) light have been investigated. The excitation spectra of these phosphors show the strongest absorption at about 395 nm, which matches well with the commercially available n-UV-emitting GaN-based LED chip. The emission spectra indicate an intense red emission due to the $^5D_0 \rightarrow {}^7F_2$ transition of Eu^{3+}, with local minima in the intensity at $Na_{0.286}Eu_{0.571}MoO_4$ and $Na_{0.200}Eu_{0.600}MoO_4$ for ~613 nm and ~616 nm bands. The phosphor $Na_5Eu(MoO_4)_4$ shows the brightest red light emission among the phosphors in the Na_2MoO_4–$Eu_{2/3}MoO_4$ system and the maximum luminescence intensity of $Na_5Eu(MoO_4)_4$ (λ_{ex} = 395 nm) in the $^5D_0 \rightarrow {}^7F_2$ transition region is close to that of the commercially used red phosphor $YVO_4:Eu^{3+}$ (λ_{ex} = 326 nm). Electron energy loss spectroscopy measurements revealed the influence of the structure and Na/Eu cation distribution on the number and positions of bands in the UV-optical-infrared regions of the EELS spectrum.

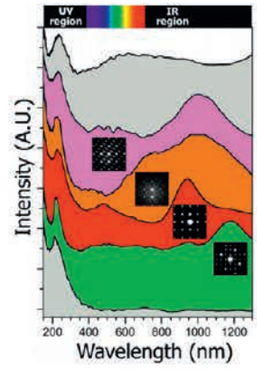

1. INTRODUCTION

White light-emitting diodes (WLEDs) receive a lot of attention as promising solid-state lighting sources, because of their high reliability, long lifetime, low energy consumption, and environmentally friendly characteristics.[1] WLEDs are used as white light sources to replace traditional incandescent and fluorescent lamps, backlights for portable electronics, medical, architecture lightings, etc.[2] Phosphor-converted WLEDs can be made by using blue/green/red tricolor phosphors excited by a near-ultraviolet (UV) (360–410 nm) InGaN-based LED and are competitive for applications that require a high quality of light (high color-rendering index, high color reproducibility, etc.).

Molybdate and tungstate phosphors have broad and intense absorption bands in the near-UV region due to charge transfer from oxygen to the metal (Mo or W). Rare earth doped molybdates and tungstates with a scheelite-type ($CaWO_4$) structure, such as $MR(BO_4)_2$ (M = Li, Na, K, Ag; R = lanthanides (Ln), Y, Bi; B = W, Mo), have shown potential as WLED[3−8] and laser materials.[9−12] For example, $NaY_{0.95}Eu_{0.05}(WO_4)(MoO_4)$,[3] $NaEu(WO_4)_2$[13] and $KGd_{0.75}Eu_{0.25}(MoO_4)_2$[14] show a much higher light output than $Y_2O_2S:Eu^{3+}$, often used as red phosphor for WLEDs.

The scheelite-type ABO_4 structure is built up by [...–AO_8–BO_4– ...] columns along the *c*-axis (Figure 1), which consist of AO_8 polyhedra and BO_4 tetrahedra sharing common vertices and forming a 3D framework. The $CaWO_4$ scheelite has tetragonal symmetry (space group $I4_1/a$).[15] The substitution of Ca^{2+} in $CaBO_4$ (B = W, Mo) by a combination of M^+ (M^+ = Li, Na) and R^{3+} (R = Ln, Y, Bi) leads to the formation of $M_xR_y(BO_4)_z$ (B = W, Mo) tungstates or molybdates. For a long time only three types of scheelite-type compounds were known in the Na_2MoO_4–$Ln_{2/3}MoO_4$ system (Ln = rare-earth elements, Y, Bi): $Na_5Ln(MoO_4)_4$ ($Na_4Ln[Na(MoO_4)_4]$),[8,16−19] $M_{0.5}R_{0.5}BO_4$[4,10−12,20−26] with a random distribution of Na^+ and Ln^{3+} cations and $Na_{1/8}Ln_{5/8}\square_{1/4}MoO_4$ ((Na + Ln)/MoO_4 ratio = 3:4; □ = cation vacancy) with a deficit in the cation

[†]Chemistry Department, Moscow State University, 119991 Moscow, Russia
[‡]Institute of Solid State Physics, 142432 Chernogolovka, Russia
[§]Laboratoire CRISMAT, UMR 6508 CNRS ENSICAEN, 6bd Maréchal Juin, 14050 Caen, France
[∥]EMAT, University of Antwerp, Groenenborgerlaan 171, B-2020 Antwerp, Belgium

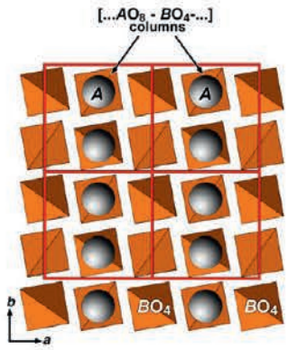

Figure 1. (Color online.) *ab* projection of the scheelite-type structure.

sublattice.[27,28] Recently, the combination of transmission electron microscopy (TEM) and X-ray diffraction (XRD) has allowed us to gather new information about the real structure of scheelite-type compounds.[29−32] A detailed analysis of the satellite reflections located between main reflections on the electron diffraction (ED) patterns has revealed that scheelite-type structures are often incommensurately modulated and require using the superspace $(3 + n)$-dimensional formalism[33] to index them.

It was shown by TEM that the real $Na_{2/7}Gd_{4/7}MoO_4$ structure is not the well-known tetragonal structure (space group $I4_1/a$) with a random distribution of Na^+ and Gd^{3+} in the *A* position as it was thought earlier. $Na_{2/7}Gd_{4/7}MoO_4$ has a (3 + 2)-dimensional ((3 + 2)D) incommensurately modulated structure with a partially ordered distribution of vacancies, Na and Gd cations.[32] On the other hand, an investigation of the $Na_xEu^{3+}{}_{(2-x)/3}\square_{(1-2x)/3}MoO_4$ ($0.015 \leq x \leq 0.5$) phases by powder X-ray diffraction (PXRD) using synchrotron radiation did not reveal the formation of any (3 + 2)D structure in the system $Na_2MoO_4-Eu_{2/3}MoO_4$.[34] Six $Na_xEu^{3+}{}_{(2-x)/3}\square_{(1-2x)/3}MoO_4$ phases ($0.015 \leq x \leq 0.25$) have a (3 + 1)D structure with different amounts of Eu^{3+} dimers while no satellite reflections have been found on the synchrotron PXRD patterns for $x = 0.5$ ($Na_{0.5}Eu_{0.5}MoO_4$) and $x = 0.286$ ($Na_{0.286}Eu_{0.571}MoO_4$ or $Na_{2/7}Eu_{4/7}MoO_4$). Therefore, the structure of $Na_{0.5}Eu_{0.5}MoO_4$ and $Na_{0.286}Eu_{0.571}MoO_4$ was refined in the conventional 3D space group with a random distribution of Na^+ and Eu^{3+} cations. The absence of satellite reflections on the synchrotron PXRD patterns for $Na_{0.286}Eu_{0.571}MoO_4$ while $Na_{0.286}Gd_{0.571}MoO_4$ is (3 + 2)D incommensurately modulated demands a detailed TEM investigation of the phases in the $Na_2MoO_4-Eu_{2/3}MoO_4$ system.

Using a detailed TEM investigation we show that also in the $Na_xEu^{3+}{}_{(2-x)/3}\square_{(1-2x)/3}MoO_4$ system (3 + 2)D incommensurately modulated phases are present; we also determine the luminescent properties of the different phases and prove with electron energy loss spectroscopy (EELS) that the dimensionality influences the luminescent properties.

2. EXPERIMENTAL SECTION

Materials and Sample Preparation. The $Na_5Eu(MoO_4)_4$ molybdenum oxide was prepared from a stoichiometric mixture of Na_2MoO_4, Eu_2O_3 (99.99%), and MoO_3 (99.99%) by the solid-state method at 923 K for 48 h. Earlier, Guo C. et al.[8] studied the influence of the annealing temperature on the stability and luminescent properties of $Na_5La(MoO_4)_4:Eu^{3+}$. It has been found that an annealing temperature in the range from 873 to 923 K is optimal for the red emission intensity of Eu^{3+} and that increasing the temperature up to 973 K leads to partial decomposition of $Na_5La(MoO_4)_4$. Cubic Na_2MoO_4 was prepared from a stoichiometric mixture of Na_2CO_3 and MoO_3 by the solid-state method at 923 K for 24 h. The monoclinic α-modification of $Eu_{2/3}MoO_4$ and $Na_xEu^{3+}{}_{(2-x)/3}\square_{(1-2x)/3}MoO_4$ ($0.138 \leq x \leq 0.5$) was synthesized by solid-state method at 1023 K for 48 h in air followed by quenching from $T = 1023$ K to room temperature (T_R). A TEM study of $Na_xEu^{3+}{}_{(2-x)/3}\square_{(1-2x)/3}MoO_4$ ($0.138 \leq x \leq 0.5$) was performed on the same samples as the ones that were studied by synchrotron PXRD.[34]

Characterization. The element composition of $Na_5Eu(MoO_4)_4$ was confirmed by energy dispersive X-ray (EDX) analysis. EDX analysis and electron diffraction (ED) were performed using a Philips CM20 microscope with an Oxford INCA attachment. The EDX analysis results were based on the Eu_L and Mo_L lines in the spectra. EDX analysis is carried out at 4 points for 10 different crystallites, in combination with ED analysis. The cation ratio has been found to be Mo/Eu = 4.04(0.35):1 (80.1 ± 1.5 at% Mo, 19.9 ± 1.5 at% Eu). This is close to the bulk $Na_5Eu(MoO_4)_4$ composition. The element content of $Na_xEu^{3+}{}_{(2-x)/3}\square_{(1-2x)/3}MoO_4$ ($0.138 \leq x \leq 0.5$) was determined earlier by inductively coupled plasma optical emission spectrometry (ICP-OES), and the Na/Eu ratios for these $Na_xEu^{3+}{}_{(2-x)/3}\square_{(1-2x)/3}MoO_4$ phases are listed in ref 34.

Samples for transmission electron microscopy were prepared by crushing powders in an agate mortar and dispersing them in methanol. A few drops of the suspension were placed on a copper grid with holey carbon film. ED and high-resolution transmission electron microscopy (HRTEM) were carried out with a JEOL 4000EX microscope operated at 400 kV and having 0.17 nm point resolution.

Electron energy loss (EELS) spectroscopy measurements were acquired on a Titan^3 80-300 operated at 80 kV equipped with a monochromator giving an energy resolution of 130 meV (full width at half-maximum of the zero-loss peak). A dispersion of 0.01 eV/pixel and an exposure time of 0.2 ms were used. Thin areas of each sample were chosen in order to avoid plural scattering. The tail of the Zero Loss was removed by subtraction of the second order polynomial fit performed in the wavelength regime.

Optical spectroscopic studies were carried out on a setup consisting of two monochromators MDR-4 and MDR-6 (wavelength range 200−1000 nm, dispersion 1.3 nm/mm), a photoelectric multiplier FEU-106 (spectral sensitivity in the range 220−800 nm), and a recording system. The MDR-4 monochromator was used to analyze the luminescence excitation spectra of the samples in the wavelength range 275−500 nm (4.51−2.48 eV). The MDR-6 monochromator was used for studying the luminescence spectra of the samples. A DKSSh-150 xenon lamp served as the light source. Photoluminescence spectra of all samples were measured under nearly the same condition to reduce the error. All measurements were performed at T_R and corrected for the sensitivity of the spectrometer.

3. RESULTS AND DISCUSSION

3.1. Electron Diffraction Study. *$Na_5Eu(MoO_4)_4$ Phase (Na/Eu Ratio = 5:1).* ED patterns of $Na_5Eu(MoO_4)_4$ along some of the main zone axes are shown in Figure 2. All strong reflections in the ED patterns can be indexed using the scheelite tetragonal $I4_1/a$ cell with unit cell parameters $a_s \approx 0.517$ nm and $c_s \approx 1.15$ nm (*s* refers to the scheelite-type unit cell) (Figure 2b). The appearance of lower intensity superstructure reflections in the [001] ED pattern necessitates the use of a supercell to be able to index all reflections.[17−19]

All reflections can be indexed in the tetragonal $I4_1/a$ space group with unit cell parameters $a \approx 1.156$ nm, $c_s \approx 1.149$ nm (Figure 2a). Thereby, $Na_5Eu(MoO_4)_4$ exhibits a structure similar to other $Na_5Ln(MoO_4)_4$ ($Na_4Ln[Na(MoO_4)_4]$) compounds[8,16−19] and is characterized by an ordered replacement of part of the anionic $[MoO_4]$ groups by Na^+ cations. However, inspired by the example of $Na_5Y(MoO_4)_4$ by Arakcheeva and Chapuis,[33] all reflections observed for $Na_5Eu(MoO_4)_4$ can also

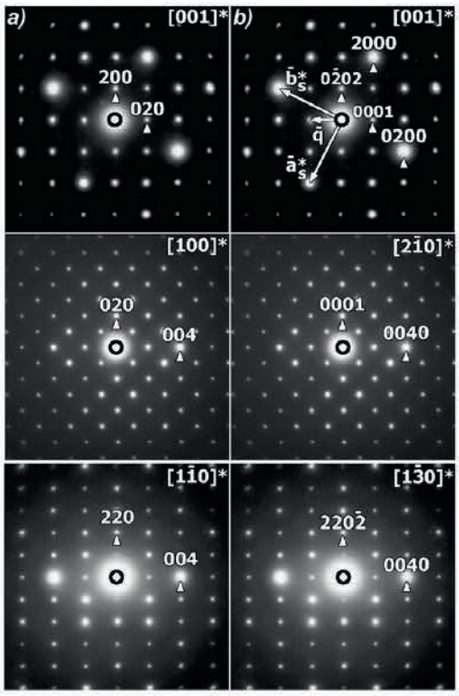

Figure 2. ED patterns along the main zone axes for $Na_5Eu(MoO_4)_4$: (a) indexed in the $I4_1/a$ tetragonal unit cell; (b) indexed in the superspace group $I2/b(\alpha\beta0)00$.

be indexed as a commensurately modulated scheelite-related structure with four *hklm* indexes given by the diffraction vector $\mathbf{H} = h\mathbf{a}^* + k\mathbf{b}^* + l\mathbf{c}^* + m\mathbf{q}$, using the superspace group (SSG) $I2/b(\alpha\beta0)00$ with unit cell parameters $a_s \approx b_s \approx 0.517$ nm, $c_s \approx 1.149$ nm, $\gamma \approx 90°$ and modulation vector $\mathbf{q} = 2/5\mathbf{a}^* + 4/5\mathbf{b}^*$, as shown in Figure 2b.

$Na_{0.138}Eu_{0.621}MoO_4$ Phase (Na/Eu Ratio = 1:4.5). The [001], [010], and [1$\bar{1}$0] ED patterns of $Na_{0.138}Eu_{0.621}MoO_4$ (Figure 3) are very similar to those reported previously for $Ag_{1/8}Pr_{5/8}MoO_4$ with a (3 + 1)D incommensurately modulated structure[29] and require a single modulation vector with two irrational components to index all satellite reflections. The most intense reflections in the [001], [010], and [1$\bar{1}$0] ED patterns are the subcell reflections; they can be indexed using the tetragonal scheelite unit cell with parameters $a_s \approx 0.52$ nm and $c_s \approx 1.15$ nm. Weaker reflections observed in the [001] ED pattern are satellite reflections, which can be indexed using indices *hklm* (as defined above) with a modulation vector $\mathbf{q} = 0.59\mathbf{a}^* - 1.21\mathbf{b}^*$ (Figure 3) and $m \neq 0$. The modulation vector $\mathbf{q}$ taken from the ED patterns is close to the modulation vector $\mathbf{q} = 0.5860(5)\mathbf{a}^* - 1.2033(1)\mathbf{b}^*$ determined from the synchrotron powder XRD patterns.[34] A more obvious choice of modulation vector would be $\mathbf{q} = 0.59\mathbf{a}^* + 0.79\mathbf{b}^*$; however, the vector $\mathbf{q} = 0.59\mathbf{a}^* - 1.21\mathbf{b}^*$ has been chosen in the published refinements from synchrotron XRPD, to which the current TEM results are compared.[34] The two vectors are related as $(\alpha,\beta,0) - (\alpha,\beta-2,0)$ and this transformation does not affect the (3 + 1)D space symmetry. Formally, it shifts the crenel domains by $x_4 = 1/2$ which does not affect the compositional modulations. Thus, the two vectors lead to an identical (3 + 1)D description of the crystal structure and can be equally used. The reflection conditions *hklmn*: $h + k + l = 2n$ and *hk0mn*: $h, k = 2n$ are in agreement with the (3 + 1)D superspace group $I2/b(\alpha\beta0)00$ (15.1.4.1 in the in the Stokes–Campbell–van Smaalen notations, $B2/b(\alpha\beta0)00$ in a standard setting[35]). All ED patterns (Figure 3) of $Na_{0.138}Eu_{0.621}MoO_4$ can be completely indexed in the $I2/b(\alpha\beta0)00$ SSG with the unique *c* axis and unit cell parameters determined earlier from the synchrotron PXRD pattern.[34]

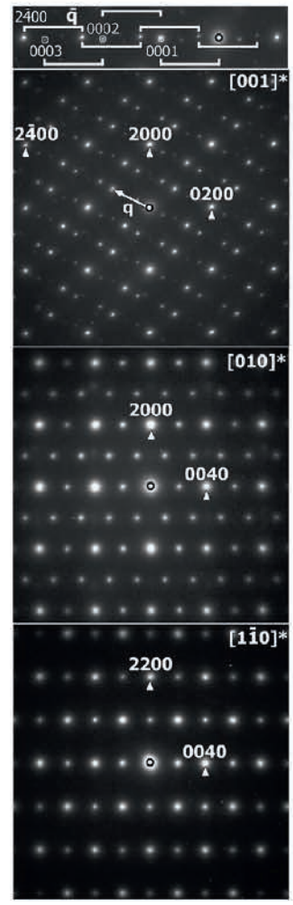

Figure 3. ED patterns along the main zone axes for the incommensurately modulated $Na_{0.138}Eu_{0.621}MoO_4$ phase and the indexation scheme of the [001] ED pattern (top).

Figure 4 shows a [001] ED pattern of $Na_{0.138}Eu_{0.621}MoO_4$ which is the superposition of two [001] ED patterns of $Na_{0.138}Eu_{0.621}MoO_4$ twinned domains rotated along the *c* axis over 90° with respect to each other. Remark that only the satellite reflections allow to detect the formation of twins in the crystal. As a consequence of the insignificant difference in the unit cell parameters and the very small deviation of the monoclinic γ-angle from 90° ($a = 0.52318$ nm, $b = 0.52310$ nm, and $\gamma = 90.232°$),[34] the positions of the main reflections are (within the limited resolution on the ED patterns) not different for the domains after rotation by 90°. White rectangles in Figure 4 based on the first order (0001 and 2$\bar{2}$0$\bar{1}$) and second order (2$\bar{2}$0$\bar{2}$) satellites for the two domains clearly show the rotation of the domains by 90°. The deviation of the monoclinic γ-angle from 90° results in the splitting of some low-intensity spots. Furthermore, the intensity of the satellite reflections for the second domain is much less than for the first domain, suggesting different amounts of both domains. The schematic drawing is shown in Figure 4b.

$Na_xEu_{(2-x)/3}\square_{(1-2x)/3}MoO_4$ Phases (x = 0.5, 0.286 (Na/Eu ~ 1:2), 0.200 (Na/Eu ~ 1:3)). [001] ED patterns of the $Na_xEu_{(2-x)/3}\square_{(1-2x)/3}MoO_4$ phases ($x = 0.5$, 0.286, 0.200) are shown in Figure 5.

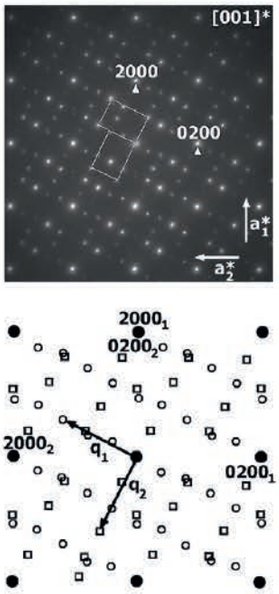

Figure 4. Superposition of [001] ED patterns for two $Na_{0.138}Eu_{0.621}MoO_4$ domains due to the 90° rotating twinning along *c* axis and schematic representation of the diffraction pattern (1 and 2 refer to the first and second domains). Full circles are main reflections; rings are satellite reflections of the first domain; squares are satellite reflections of the second domain.

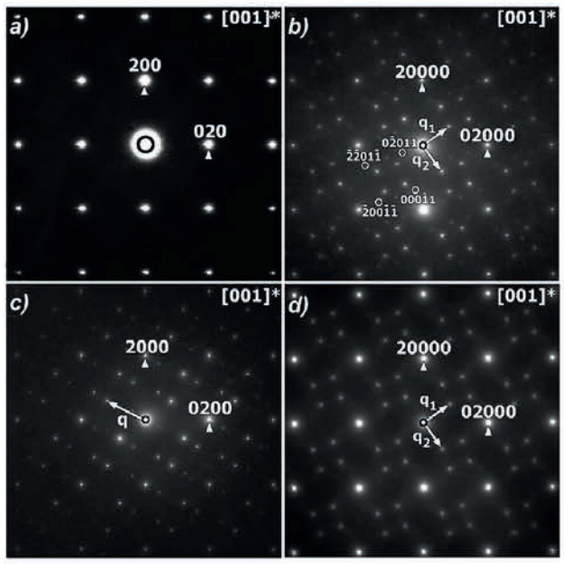

Figure 5. [001] ED patterns of $Na_xEu^{3+}{}_{(2-x)/3}\square_{(1-2x)/3}MoO_4$ phases (x = 0.5 (*a*), 0.286 (*b*), 0.200 (*c*, *d*)). White rings mark *hk*0*mn* reflections with $|m| = |n| = 1$.

In the [001] ED pattern of $Na_{0.5}Eu_{0.5}MoO_4$ (Figure 5*a*), no weaker reflections are observed, in contrast to other phases in the Na_2MoO_4–$Eu_{2/3}MoO_4$ system. All reflections can be indexed in the tetragonal scheelite $I4_1/a$ space group with unit cell parameters $a_s \approx 0.52$ nm and $c_s \approx 1.15$ nm assuming a random distribution of Na^+ and Eu^{3+} cations in the structure.

The [001] ED pattern of $Na_{0.286}Eu_{0.571}MoO_4$ is very similar to the one reported previously for $Na_{2/7}Gd_{4/7}MoO_4$ with a (3 + 2)D incommensurately modulated structure[32] and indicates that $Na_{0.286}Eu_{0.571}MoO_4$, like $Na_{2/7}Gd_{4/7}MoO_4$, has a (3 + 2)D incommensurately modulated structure with a partially ordered distribution of vacancies, Na^+ and Eu^{3+} cations. In contrast to the [001] ED pattern for the (3 + 1)D $Na_{0.138}Eu_{0.621}MoO_4$, the weaker reflections observed in the [001] ED pattern for $Na_{0.286}Eu_{0.571}MoO_4$ cannot be indexed with four digit indices *hk*0*m* but require the use of 5 digit indices *hk*0*mn*, corresponding to the diffraction wave vector $\mathbf{H} = h\mathbf{a}^* + k\mathbf{b}^* + l\mathbf{c}^* + m\mathbf{q}_1 + n\mathbf{q}_2$, with modulation vectors $\mathbf{q}_1 \approx 0.57\mathbf{a}^* + 0.80\mathbf{b}^*$ and $\mathbf{q}_2 \approx -0.80\mathbf{a}^* + 0.57\mathbf{b}^*$. The presence of reflections with m and n both equal to $\bar{1}$ or 1 on the [001] ED pattern proves that $Na_{0.286}Eu_{0.571}MoO_4$ is tetragonal with two modulation vectors (Figure 5*b*). The $\mathbf{q}_1$ and $\mathbf{q}_2$ vectors are symmetrically dependent according to the tetragonal symmetry of the underlying basic scheelite structure for this composition. The *hklmn*: $h + k + l = 2n$ and *hk*0*mn*: $h, k = 2n$ reflection conditions are in agreement with the space group $I4_1/a$ for the basic structure. Thus, the ED patterns of $Na_{0.286}Eu_{0.571}MoO_4$ can be completely indexed (similar to $Na_{2/7}Gd_{4/7}MoO_4$) in the tetragonal superspace group with unit cell parameters $a_s \approx 0.524$ nm, $c_s \approx 1.150$ nm and two modulation vectors $\mathbf{q}_1 \approx 0.57\mathbf{a}^* + 0.80\mathbf{b}^*$ and $\mathbf{q}_2 \approx -0.80\mathbf{a}^* + 0.57\mathbf{b}^*$. These ED results clearly show the presence of satellite reflections, whereas they were absent on the synchrotron PXRD data.[34] They are much weaker than those previously found for $Na_{2/7}Gd_{4/7}MoO_4$,[32] which could explain why for $Na_{0.286}Eu_{0.571}MoO_4$ they were not detected by synchrotron PXRD.

In contrast to other $Na_xEu^{3+}{}_{(2-x)/3}\square_{(1-2x)/3}MoO_4$ phases, two types of [001] ED patterns are observed for the composition with x = 0.200 (Figure 5c and d). The ED pattern in Figure 5*c* is very similar to the [001] ED pattern of $Na_{0.138}Eu_{0.621}MoO_4$ (Figure 3) and can be completely indexed using the $I2/b(\alpha\beta 0)00$ SSG with the unit cell parameters and modulation vector determined earlier from the synchrotron PXRD pattern.[34] However, other ED patterns, of which an example is shown in Figure 5*d* are similar to the [001] ED pattern of $Na_{0.286}Eu_{0.571}MoO_4$ with two modulation vectors $\mathbf{q}_1 \approx 0.55\mathbf{a}^* + 0.79\mathbf{b}^*$ and $\mathbf{q}_2 \approx -0.79\mathbf{a}^* + 0.55\mathbf{b}^*$. The reflections *hk*0*mn* with m and n both different from 0 are also present here, although much weaker than in Figure 5b.

3.2. High Resolution Transmission Electron Microscopy. HRTEM observations were performed along the most informative zone axis [001] where the structure of the $Na_xEu_{(2-x)/3}\square_{(1-2x)/3}MoO_4$ phases can be interpreted in terms of columns of A cations and MoO_4 groups. Also, among the main zones, only the [001] ED patterns exhibit superstructure reflections (Figure 3). In order to understand the origin of these superstructure reflections, HRTEM has been performed. [001] HRTEM images of the $Na_xEu_{(2-x)/3}\square_{(1-2x)/3}MoO_4$ phases (x = 0.138, 0.200) together with the corresponding ED patterns are shown in Figures 6–8, respectively. On these images the bright dots represent the projected cationic columns. Along the [001] direction, the A and B cations are projected on top of each other.

Figure 6 shows [001] HRTEM images of $Na_{0.138}Eu_{0.621}MoO_4$ and the corresponding ED patterns. Two different modulation types can be detected on the [001] HRTEM images. In the first one (Figure 6a), the variation in the brightness of the dots in the image is in agreement with the modulation vector derived from the ED patterns (Figure 3) and corresponds to the (3 + 1)D structure. The difference in brightness between the dots is clearly visible resulting in a wavy contrast due to the compositional modulation.[34] In other areas though, the modulation waves propagate along two perpendicular directions (marked with arrows) (Figure 6b). The image of the (3 + 1)D structure in Figure 6a consists of chains of four linear

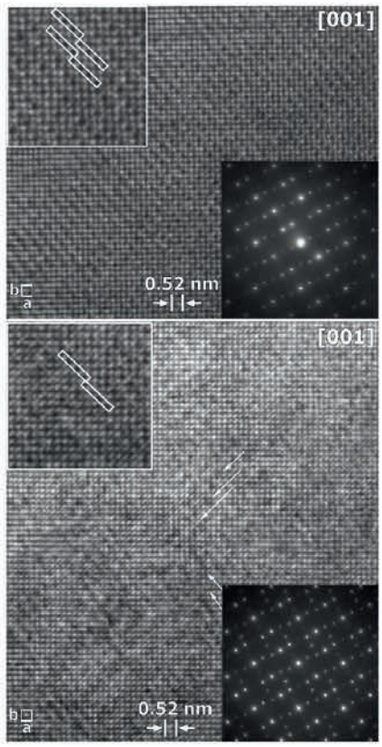

Figure 6. [001] HRTEM images of $Na_{0.138}Eu_{0.621}MoO_4$.

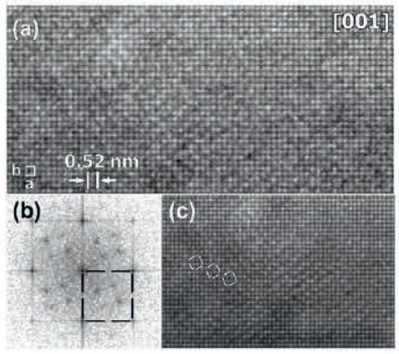

Figure 7. (a) [001] HRTEM image of $Na_{0.200}Eu_{0.600}MoO_4$; (b) Fourier transform obtained from the HRTEM image; and (c) lower magnification low pass filtered "image of a larger area around part a", using a Bragg-mask filter, basic reflections marked as the black square in part b were used to improve the signal-to-noise ratio. A thick region is shown because the modulation quickly disappears under the electron beam, thin regions first.

bright dots corresponding to [...$-AO_8-MoO_4-$ ...] columns of atoms (marked by white rectangles) along the *c*-axis, similarly oriented and shifted with respect to each other in accordance to the modulated vector. The image in Figure 6b with modulation waves along two perpendicular directions clearly consists of two families of the same chains as in Figure 6a but rotated with respect to each other over 90° and is therefore a twinned area. This observation confirms the structural model and the interpretation proposed for the ED patterns in Figure 4.

[001] HRTEM images of $Na_{0.200}Eu_{0.600}MoO_4$ are shown in Figures 7 and 8. The Fourier transforms obtained from the HRTEM image (Figures 7b and 8b) exhibit patterns similar to those of the ED patterns (Figure 5d and c), indicating that the modulation features are still present in the image (they disappear after a short time under the electron beam). In order

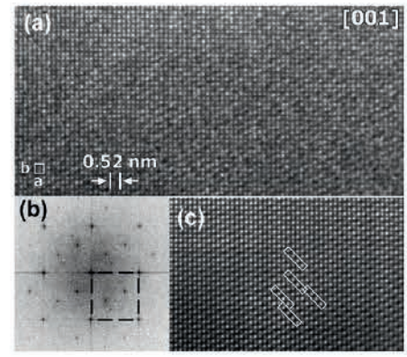

Figure 8. (a) [001] HRTEM image of $Na_{0.200}Eu_{0.600}MoO_4$; (b) Fourier transform obtained from the HRTEM image; and (c) higher magnification filtered HRTEM image of part a, using a Bragg-mask filter, basic reflections marked as the black square in part b were used to improve the signal-to-noise ratio.

to enhance the signal-to-noise ratio in the HRTEM image and clarify the nature of the satellite reflections on the ED patterns, Fourier filtering was applied using a Bragg mask. The mask size was chosen in such way that no structural information was lost and no artifacts were introduced, as proven by the persisting similarity between the filtered images (Figures 7c and 8c) and the experimental images (Figure 7a and 8a). Figures 7c and 8c show filtered HRTEM images of the $Na_{0.200}Eu_{0.600}MoO_4$ phase using the basic reflections marked with black squares in the Fourier transforms (Figures 7b and 8b).

The [001] HRTEM image of $Na_{0.200}Eu_{0.600}MoO_4$ shown in Figure 7 consists of square blocks of brighter dots (marked by a white square) containing inside four dots with lower intensity. Previously such type of blocks were observed on the [001] HRTEM image of $Na_{2/7}Gd_{4/7}MoO_4$.[32] The shift of the blocks of brighter dots relative to each other along two perpendicular directions corresponds to the satellite reflections on the ED pattern (Figure 5d). Thus, the HRTEM image confirms that the fragment of the $Na_{0.200}Eu_{0.600}MoO_4$ structure shown in Figure 7 is (3 + 2)-dimensionally modulated, and not simply twinned, since the modulation waves propagate along two perpendicular directions in all observed areas and both modulation vectors $\mathbf{q}_1$ and $\mathbf{q}_2$ are clearly present on the Fourier transform (Figure 7b). The [001] HRTEM image of a second fragment of the $Na_{0.200}Eu_{0.600}MoO_4$ structure (Figure 8c) is similar to the [001] HRTEM image of the (3 + 1)D $Na_{0.138}Eu_{0.621}MoO_4$ (Figure 6a). It also consists of chains of four linear bright dots, similarly oriented and shifted with respect to each other in accordance with the modulation vector. In conclusion, two types of modulated structures have been found for $Na_{0.200}Eu_{0.600}MoO_4$: a (3 + 1)D incommensurately modulated structure and a (3 + 2)D incommensurately modulated one. The change from (3 + 1)D to (3 + 2)D here involves the occurrence of a second modulation vector perpendicular to the one in the (3 + 1)D structure, with the same length.

3.3. Luminescent Properties. The photoluminescent excitation (PLE) and the photoluminescent emission (PL) spectra of the $Na_5Eu(MoO_4)_4$ and $Na_{0.5}Eu_{0.5}MoO_4$ phosphors are shown in Figures 9 and 10. The PLE spectrum of $Na_{0.5}Eu_{0.5}MoO_4$, shown in Figure 9b, is representative for all $Na_xEu^{3+}_{(2-x)/3}\square_{(1-2x)/3}MoO_4$ ($0.138 \leq x \leq 0.5$) phases. The PL spectra of all phases are shown in Figure 11. Positions and intensities of two maximum bands on the PL and PLE spectra

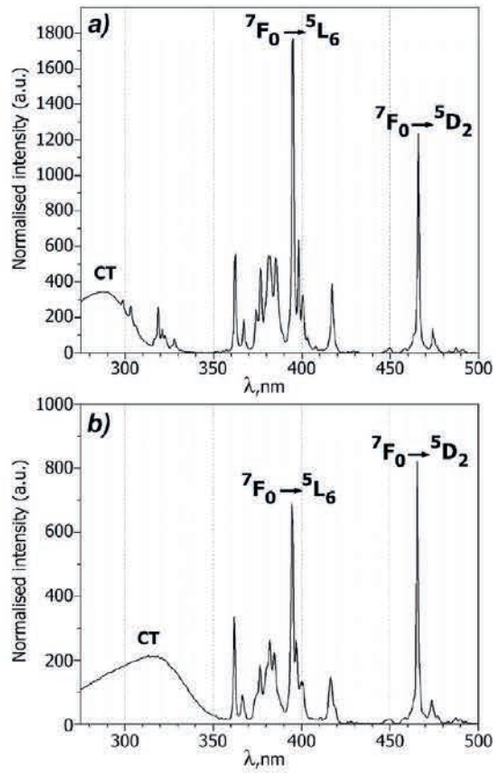

Figure 9. PLE spectra of $Na_5Eu(MoO_4)_4$ (a) (λ_{em} = 617.4 nm) and $Na_{0.5}Eu_{0.5}MoO_4$ (b) (λ_{em} = 615.6 nm).

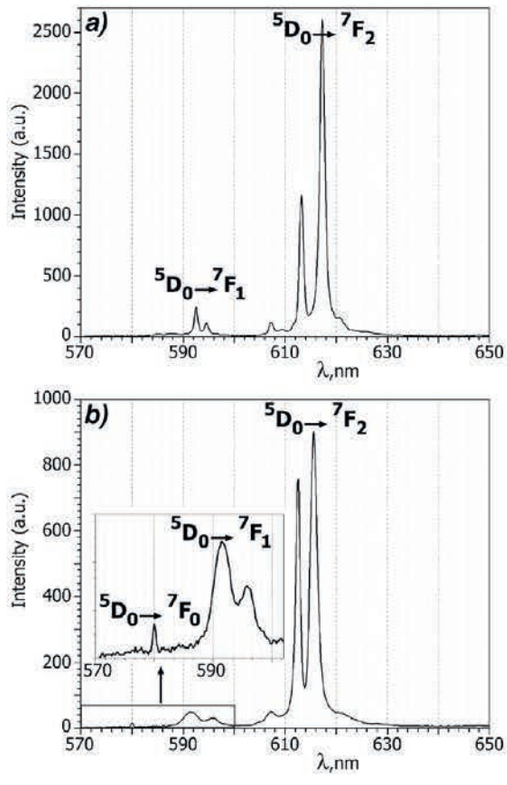

Figure 10. PL (λ_{ex} = 395 nm) spectra of $Na_5Eu(MoO_4)_4$ (a) and $Na_{0.5}Eu_{0.5}MoO_4$ (b).

of phases in the Na_2MoO_4–$Eu_{2/3}MoO_4$ system are given in Table 1.

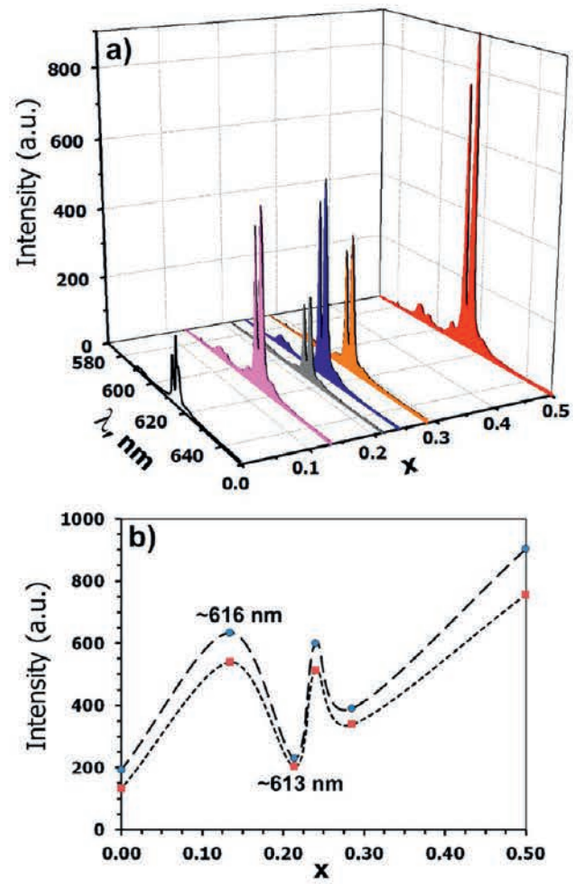

Figure 11. (Color online.) PL (λ_{ex} = 395 nm) spectra of $Na_xEu^{3+}{}_{(2-x)/3}\square_{(1-2x)/3}MoO_4$ ($0 \le x \le 0.5$) (a) and the concentration dependence of the $^5D_0 \rightarrow {}^7F_2$ emission for $\lambda_{max}(1)$ ~613 nm and $\lambda_{max}(2)$ ~616 nm bands on x (b). All samples were measured under the same conditions.

As shown in Figure 9, the PLE spectra were measured in the spectral range from 275 to 500 nm by monitoring the emission at 617.4 nm and 615.6 nm, which is attributed to the $^5D_0 \rightarrow {}^7F_2$ transition of Eu^{3+} ions. Both PLE excitation spectra show a broad excitation band in the range 275–300 nm and 275–350 nm as well as a group of sharp lines in the range 300–500 nm and 350–500 nm for $Na_5Eu(MoO_4)_4$ and $Na_{0.5}Eu_{0.5}MoO_4$, respectively. The broad excitation bands centered at ~290 nm for $Na_5Eu(MoO_4)_4$ (Figure 9a) and at ~315 nm for $Na_{0.5}Eu_{0.5}MoO_4$ (Figure 9b) are attributed to a charge transfer (CT) from oxygen to molybdenum inside the MoO_4^{2-} groups. In the spectral region from 350 to 500 nm all phases in the Na_2MoO_4–$Eu_{2/3}MoO_4$ system show characteristic intraconfigurational 4f–4f emissive transitions of Eu^{3+}: a sharp $^7F_0 \rightarrow {}^5L_6$ transition for 394.5–395 nm, a $^7F_0 \rightarrow {}^5D_2$ transition for 465.5–466 nm (Table 1). In accordance with Table 1 and Figure 9, the change of the crystal structure from $Na_5Eu(MoO_4)_4$ to $Na_{0.5}Eu_{0.5}MoO_4$ practically does not change positions of the bands of $^7F_0 \rightarrow {}^5L_6$ and $^7F_0 \rightarrow {}^5D_2$ transitions but leads to a decreasing intensity of these bands, changing of the $^7F_0 \rightarrow {}^5L_6/{}^7F_0 \rightarrow {}^5D_2$ ratio and a shift of the center of the broad excitation band toward longer wavelengths.

PL spectra of $Na_5Eu(MoO_4)_4$ and $Na_xEu_{(2-x)/3}\square_{(1-2x)/3}MoO_4$ ($0.138 \le x \le 0.5$) phases are shown in Figures 10 and 11. PL spectra in the spectral range from 570 to 650 nm show the typical red emitting features of

Table 1. Positions (λ_{max}) and Intensities (I_{max}) of Two Maximum Bands on PL and PLE Spectra of Phases in the Na_2MoO_4–$Eu_{2/3}MoO_4$ System[a]

	PL spectra				PLE spectra			
	$^5D_0 \rightarrow {}^7F_2$				$^7F_0 \rightarrow {}^5L_6$		$^7F_0 \rightarrow {}^5D_2$	
phase	$\lambda_{max}(1)$, nm	$I_{max}(1)$	$\lambda_{max}(2)$, nm	$I_{max}(2)$	$\lambda_{max}(1)$, nm	$I_{max}(1)$	$\lambda_{max}(2)$, nm	$I_{max}(2)$
$Na_5Eu(MoO_4)_4$	613.4	1156	617.4	2605	395	1767	466	1236.8
$Na_{0.5}Eu_{0.5}MoO_4$	612.6	756.4	615.6	903.4	394.5	689.9	465.5	819.8
$Na_{0.286}Eu_{0.571}MoO_4$	612.6	338.1	615.6	390	394.5	256.3	465.5	303.7
$Na_{0.240}Eu_{0.587}MoO_4$	612.6	513	615.6	599.8	394.5	474.8	465.5	565.6
$Na_{0.200}Eu_{0.600}MoO_4$	612.8	202.7	615.8	230.5	394.5	176.1	465.5	205.8
$Na_{0.138}Eu_{0.621}MoO_4$	612.6	538.3	615.6	633.6	394.5	505.3	465.5	600.7
$Eu_{2/3}MoO_4$	613.2	132.6	615.6	193.2				

[a]All samples are measured under the same conditions.

Eu^{3+}, including $^5D_0 \rightarrow {}^7F_J$ (J = 0, 1, 2) emissions. The most intense peak in the region from 600 to 620 nm is due to the electric dipole transition $^5D_0 \rightarrow {}^7F_2$. $^5D_0 \rightarrow {}^7F_2$ transition bands at ~613 nm and at ~616 nm on the PL spectrum of $Na_5Eu(MoO_4)_4$ have more intensity than those of all $Na_xEu^{3+}{}_{(2-x)/3}\square_{(1-2x)/3}MoO_4$ ($0.138 \le x \le 0.5$) phases (Figure 10, Table 1). The transition at 590 nm is the $^5D_0 \rightarrow {}^7F_1$ magnetic dipole transition. Emission wavelengths of these 4f–4f transitions are only moderately influenced by the environment of the lanthanide ions since the partially filled 4f shell is well shielded by the filled 5s and 5p orbitals. Nevertheless, it is possible to correlate the spectrum with the symmetry of the site.

$CaWO_4$ with the tetragonal symmetry (space group $I4_1/a$) has C_{4h} as 3D point group. The Ca–O distances in the CaO_8 polyhedron vary from 0.2450 to 0.2486 nm (difference between the distances of 1.5%). The substitution of Ca^{2+} in $CaMoO_4$ by Na^+ and R^{3+} (R = Ln, Y, Bi) leads to the formation of double molybdates $Na_5R(MoO_4)_4$ and $Na_{0.5}R_{0.5}MoO_4$ with ordering or random distribution of Na^+ and R^{3+} cations, respectively. Both types of compounds also have the tetragonal symmetry (space group $I4_1/a$) and C_{4h} as 3D point group. However, the distortion of the RO_8 polyhedron is different for both compounds and much larger for $Na_{0.5}R_{0.5}MoO_4$. For example, the La–O distances in the LaO_8 polyhedron in $Na_5La(MoO_4)_4$ [17] and $NaLa(MoO_4)_2$[36] vary from 0.2495 to 0.2498 nm (difference between the distances of 0.1%) and from 0.2559 to 0.2616 nm (a difference of 2.2%), respectively.

Due to the distortion of the RO_8 polyhedron for $Na_xEu^{3+}{}_{(2-x)/3}\square_{(1-2x)/3}MoO_4$ ($0.138 \le x \le 0.5$) structures, the Na^+ and R^{3+} cations occupy a site with maximal C_2 site symmetry. The lack of inversion symmetry induces a high intensity of the hypersensitive $^5D_0 \rightarrow {}^7F_2$ transition. Another consequence is the appearance of a band of the $^5D_0 \rightarrow {}^7F_0$ transition at 580 nm on the PL spectra of the $Na_xEu^{3+}{}_{(2-x)/3}\square MoO_4$ ($0.138 \le x \le 0.5$) phases (Figure 10 and 11). Since the $^5D_0 \rightarrow {}^7F_0$ transition is forbidden both for electric and magnetic dipole interactions, the intensity can be very low or even nonobservable. Yet, for C_2 symmetry the transition is induced, so a peak can be expected at that position. As splitting of the initial and final level, both characterized by J = 0, is not possible, observing more than one transition would be an indication of the presence of more than one nonequivalent site for the luminescent Eu^{3+} ions. Since we observe only one peak for all $Na_xEu^{3+}{}_{(2-x)/3}\square_{(1-2x)/3}MoO_4$ ($0.138 \le x \le 0.5$) phases, the local environment of the Eu^{3+}ions probably remains the same over the whole crystal.[37]

Figure 11 shows PL spectra (λ_{ex} = 395 nm) of $Na_xEu^{3+}{}_{(2-x)/3}\square_{(1-2x)/3}MoO_4$ ($0 \le x \le 0.5$) and the concentration dependence of the $^5D_0 \rightarrow {}^7F_2$ emission for ~613 nm and ~616 nm bands on x. The intensity of the Eu^{3+} emission decreases with decreasing Na^+ content (x) from 0.5 to 0 but two local minima are observed for x = 0.286 and x = 0.200 (Figure 11b). Earlier, such local minima at x = 0.286 and x = 0.200 were observed in the dependencies of the characteristic parameters of the Eu^{3+}-centered luminescence (overall quantum yields (Q_L^{Eu}), observed lifetimes (τ_{obs}), intrinsic quantum yields (Q_{Eu}^{Eu})) of $Na_xEu^{3+}{}_{(2-x)/3}\square_{(1-2x)/3}MoO_4$ ($0.015 \le x \le 0.5$) phases on the Eu^{3+} concentration.[34]

Based on the refinement of six (3 + 1)D incommensurately modulated structures of $Na_xEu^{3+}{}_{(2-x)/3}\square_{(1-2x)/3}MoO_4$ phases ($0.015 \le x \le 0.25$) with the ordered distribution of vacancies, Na and Eu cations, a correlation has been proposed between the relative amount of Eu^{3+} dimers and the characteristic parameters (Q_L^{Eu}, Q_{Eu}^{Eu}, τ_{obs}) of the Eu^{3+}-centered luminescence.[34] At the same time, it was believed that $Na_xEu_{(2-x)/3}{}^{3+}\square_{(1-2x)/3}MoO_4$ phases with x = 0.286 and x = 0.5 have 3D nonmodulated structures with one crystallographic cation position statistically occupied by Eu^{3+} and Na^+. However, our detailed TEM study has revealed that $Na_{0.286}Eu_{0.571}MoO_4$ has a (3 + 2)D incommensurately modulated structure, such as the $Na_{2/7}Gd_{4/7}MoO_4$ structure,[32] in which there is a full ordering of vacancies and a partially ordered distribution of Eu^{3+} and Na^+ cations. In addition, similar domains with the (3 + 2)D structure have been found next to (3 + 1)D domains in $Na_{0.200}Eu^{3+}{}_{0.600}MoO_4$. Thus, the occurrence of the (3 + 2)D modulation coincides with the local minima in the luminescence properties.

There are two possible reasons for the decreasing $^5D_0 \rightarrow {}^7F_2$ emission intensity of $Na_xEu_y(MoO_4)_z$ red phosphors (Figures 10 and 11) as the Na/Eu ratio varies from 5:1 to 1:2. 1) A quenching effect because usually the luminescent intensity decreases with increasing concentration of the luminescent centers; 2) changing the structure from 3D with an ordered distribution of Eu^{3+} and Na^+ cations (Na/Eu = 5:1) to a (3 + 2)D incommensurately modulated structure with a partially ordered distribution (Na/Eu = 1:2) via a 3D structure for Na/Eu = 1:1 with a random distribution of Eu^{3+} and Na^+ cations.

Concentration quenching is caused by the energy transfer between luminescent centers, and these energy-transfer chains trigger the energy migration to the energy sink such as crystalline defects or trace ions. As the concentration of Eu^{3+} ions increases, the distance between the Eu^{3+} ions decreases

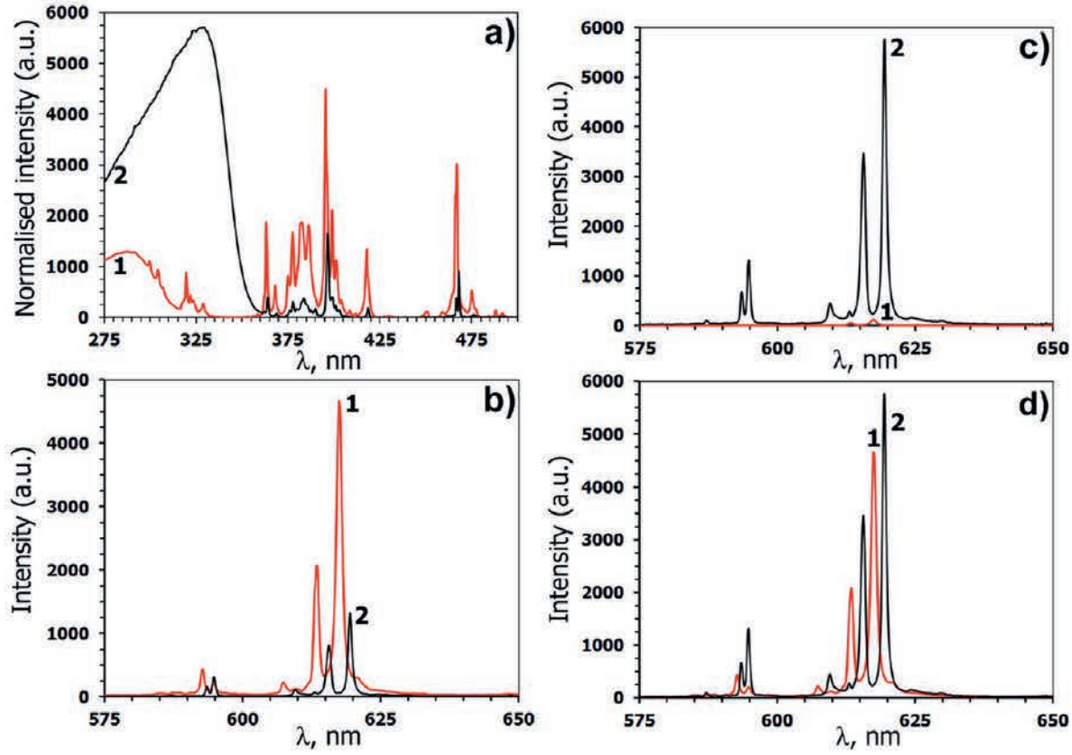

Figure 12. (Color online.) Spectra of $Na_5Eu(MoO_4)_4$ (1) and $YVO_4:Eu^{3+}$ (2): PLE spectra of $Na_5Eu(MoO_4)_4$ (λ_{em} = 617.4 nm) and $YVO_4:Eu^{3+}$ (λ_{em} = 619.2 nm) (a); PL spectra (λ_{ex} = 395 nm (b) and λ_{ex} = 326 nm (c)), (d) PL spectra of $Na_5Eu(MoO_4)_4$ (λ_{ex} = 395 nm) and $YVO_4:Eu^{3+}$ (λ_{ex} = 326 nm). Both samples are measured under the same conditions.

due to difference between the size of the Eu^{3+} and Na^+ cations ($r_{VIII}(Na^+)$ = 1.18 Å and $r_{VIII}(Eu^{3+})$ = 1.066 Å[38]), favoring a nonradiative energy transfer among Eu^{3+} ions. For example, the R−R distances in $Na_5R(MoO_4)_4$ (R = La,[17] Y[19]) and $Na_{0.5}R_{0.5}MoO_4$ (R = La,[36] Y[19]) vary from 0.6475 to 0.3969 nm (La−La) and from 0.6366 to 0.3844 nm (Y−Y), respectively. On one hand, the $^5D_0 \rightarrow {}^7F_2$ emission intensity of $Na_5La_{1-x}Eu_x(MoO_4)_4$[8] and $Na_{0.5}(Gd_{1-x}Eu_x)_{0.5}MoO_4$[39] solid solutions is reported to increase with an increasing concentration of Eu^{3+} ions and to reach a maximum at x = 1. On the other hand, Zhao et al.[40] found that the $^5D_0 \rightarrow {}^7F_2$ emission increases with an increase of the Eu^{3+} content up to x = 0.7 in $Na_{2/7}(Gd_{1-x}Eu_x)_{4/7}MoO_4$ solid solutions, followed by a decrease due to a concentration quenching effect. The $^5D_0 \rightarrow {}^7F_2$ emission intensity of $Na_{2/7}(Gd_{0.3}Eu_{0.7})_{4/7}MoO_4$ is about five times higher than that of $Y_2O_3:Eu^{3+}$ phosphor under blue excitations λ_{ex} = 466 nm and changing excitations from λ_{ex} = 466 nm to λ_{ex} = 396 nm does not lead to a noticeable change of the emission intensity of $Na_{2/7}(Gd_{0.3}Eu_{0.7})_{4/7}MoO_4$. The $^5D_0 \rightarrow {}^7F_2$ emission intensity of pure $Na_{2/7}Eu_{4/7}MoO_4$ is approximately 75% of the intensity for $Na_{2/7}(Gd_{0.3}Eu_{0.7})_{4/7}MoO_4$ under both excitations. Such high quenching concentrations are caused by the scheelite-related structure and are observed for other Eu^{3+}-doped molybdates. Thus, the relation between the decrease in the $^5D_0 \rightarrow {}^7F_2$ emission and the increase of the Eu^{3+} concentration in our view could be more complex than only a concentration quenching effect, since the increase of the Eu^{3+} concentration also leads to changes in the structure and in the Eu^{3+} distribution. To determine this complex relation between structure and properties, a material is required for which the reflections corresponding to the (3 + 2)D structure are observable with bulk diffraction or single crystal techniques to enable a refinement of the structures. For the current material, these reflections were only observed by electron microscopy.

The second local minimum of the Eu^{3+} emission observed on the PL spectra of $Na_xEu^{3+}{}_{(2-x)/3}\square_{(1-2x)/3}MoO_4$ ($0 \le x \le 0.5$) for x = 0.200 (Figure 11b) has been associated with the number and ordering of the Eu^{3+} dimers.[34] The successful solution of the $Na_{0.200}Eu^{3+}{}_{0.600}MoO_4$ structure as (3 + 1)D incommensurately modulated[34] indicates that this is the main phase. It cannot be excluded that the change in dimensionality anyway has an effect on the luminescence, while it can go undetected by bulk diffraction techniques, therefore these phases will be investigated using the local technique of electron energy loss spectroscopy (EELS) in the next section.

As shown in Figured 10 and 11, among the phases in the system Na_2MoO_4−$Eu_{2/3}MoO_4$, the maximum intensity of luminescence in the region from 600 to 620 nm ($^5D_0 \rightarrow {}^7F_2$ transition) is observed for $Na_5Eu(MoO_4)_4$. Concerning applications, the color chromaticity of phosphors is considered to be a critical parameter for evaluating the performance of LED phosphors. In literature, the luminescent properties of the $Na_5Eu(MoO_4)_4$ red-emitting phosphor are reported and compared against those of the commodity $Y_2O_2S:Eu^{3+}$ and $La_2O_2S:Eu^{3+}$.[41] It was found that the CIE color coordinates (x,y) and relative luminance (rl) of $Na_5Eu(MoO_4)_4$ ((x,y) = (0.66, 0.33), rl =1.3) are similar to those of $Y_2O_2S:Eu^{3+}$. Here, we compare the luminescent properties of $Na_5Eu(MoO_4)_4$ and $YVO_4:Eu^{3+}$, a well-known highly efficient red light-emitting material and an attractive phosphor because of its high luminescence quantum yield (QY).[42] Figure 12 shows the comparison of PLE and PE spectra of $Na_5Eu(MoO_4)_4$ and $YVO_4:Eu^{3+}$. As shown in Figure 12d, the maximum

luminescence intensity of $Na_5Eu(MoO_4)_4$ (λ_{ex} = 395 nm) in the $^5D_0 \rightarrow {}^7F_2$ transition region is close to the luminescence intensity of $YVO_4:Eu^{3+}$ (λ_{ex} = 326 nm). This confirms that $Na_5Eu(MoO_4)_4$ is exceptionally attractive as a near-UV convertible phosphor applied as a red-emitting phosphor for LEDs as suggested in ref 16a.

3.4. Electron Energy Loss Spectroscopy. To determine whether the change in dimensionality has an effect on the luminescent properties, a local technique such as EELS needs to be applied, which allows to correlate spectra with specific crystallites or even domains. Figure 13 shows the comparison of EELS spectra of Na_2MoO_4, $Na_5Eu(MoO_4)_4$, $Na_xEu^{3+}_{(2-x)/3}\square_{(1-2x)/3}MoO_4$ ($0.138 \leq x \leq 0.5$) and α-$Eu_{2/3}MoO_4$. EELS spectra are presented in the spectral range from 150 to 1300 nm (corresponding to the range of energy from 0.95 to 8.27 eV). Three spectral regions can be noticed: ultraviolet (<380 nm (I), visible light (from 380 to 740 nm (II)), and infrared (>740 nm(III)).

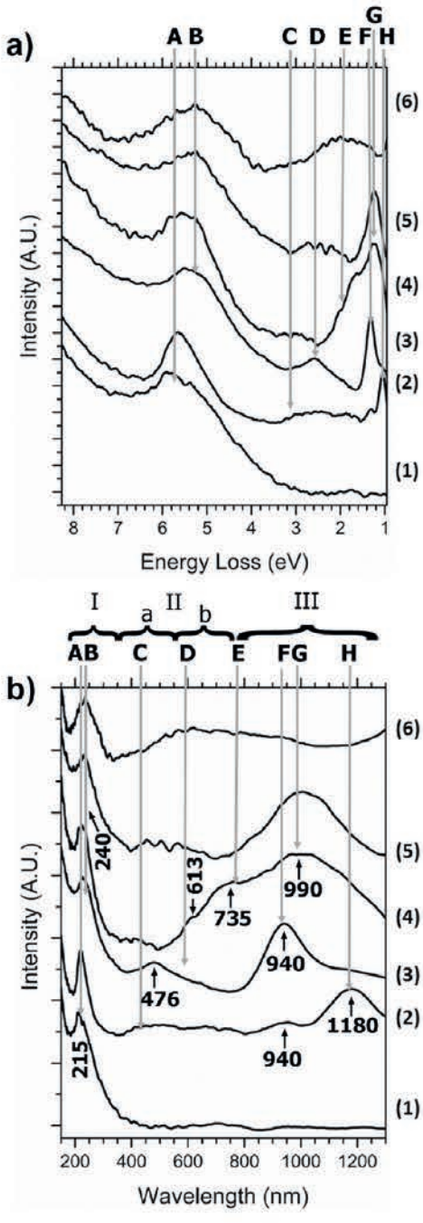

Figure 13. (a) Background subtracted EELS spectra of Na_2MoO_4 (1), $Na_5Eu(MoO_4)_4$ (2), $Na_{0.5}Eu_{0.5}MoO_4$ (3), $Na_{0.286}Eu_{0.571}MoO_4$ (4), $Na_{0.138}Eu_{0.621}MoO_4$ (5) and α-$Eu_{2/3}MoO_4$ (6) plotted as a function of energy loss. (b) Same spectra plotted in wavelength scale. (I, ultraviolet region; II, vision light (a, region of PLE spectra; b, region of PL spectra); and III, infrared region). Scales were matched for easy comparison with PLE and PL spectra.

All EELS spectra are similar in the range from 150 to 380 nm (ultraviolet region) and show only one broad absorption band. Broad absorption band positions (~215–240 nm) are close to the positions of the CT bands observed on the PLE spectra (Figure 9). These broad absorption bands can be therefore assigned to the charge transfer (CT) from oxygen to molybdenum inside the MoO_4^{2-} groups. Increasing the Eu^{3+} concentration from $Na_5Eu(MoO_4)_4$ to $Na_{0.5}Eu_{0.5}MoO_4$ leads to a clear broadening of the CT bands and a shift of the maximum from ~215 nm (A in Figure 13) to ~240 nm (B in Figure 13). A similar modification of the center of the CT bands with increasing Eu^{3+} concentration from $Na_5Eu(MoO_4)_4$ to $Na_{0.5}Eu_{0.5}MoO_4$ is observed on PLE spectra.

Peculiarities of EELS spectra of studied compounds are clearly observed in the regions of the visible light and infrared regime (Figure 13). As shown in Figure 13, the EELS spectrum of Na_2MoO_4 contains no other peaks except a broad absorption band while the EELS spectrum of α-$Eu_{2/3}MoO_4$ besides shifting the maximum of this peak from ~215 nm to ~240 nm is characterized by the presence of a second broad absorption band in the region from 350 to 1000 nm. The maximum of the second broad absorption band is about ~610 nm which is in agreement with the $^5D_0 \rightarrow {}^7F_2$ transition bands at ~613 nm and at ~616 nm on the PL spectrum (Table 1, Figure 11). The EELS spectrum of $Na_5Eu(MoO_4)_4$ in the region from 350 to 1300 nm shows the presence of three absorption bands: a first broad absorption band in the visible range and two bands at ~940 nm and at ~1180 nm in the infrared region. Changing of the Na and Eu cation distribution from ordered in $Na_5Eu(MoO_4)_4$ to random in the $Na_{0.5}Eu_{0.5}MoO_4$ structure leads to a vanishing of the band at ~1180 nm, a significant increasing intensity of the band at ~940 nm and the appearance of a new band at ~476 nm. Further increase of Eu^{3+} concentration and modification of the cation distribution due to formation of incommensurately modulated structures leads to a change in the number of bands in the spectra, broadening of the most intense band and a change in its center from ~940 nm to ~990 nm but does not lead to its disappearence. Absorption bands at ~940 nm and ~1180 nm in the infrared regime may be associated with the Eu–Eu or Eu–Na interactions, respectively. On one hand, $Na_5Eu(MoO_4)_4$ shows the maximum intensity of luminescence in the region from 600 to 620 nm ($^5D_0 \rightarrow {}^7F_2$ transition) among the $Na_xEu_y(MoO_4)_z$ red phosphors and the band at ~1180 nm in the infrared region is observed only on EELS spectrum of $Na_5Eu(MoO_4)_4$. On the other hand, the $Na_5Eu(MoO_4)_4$ structure has the longest Eu–Eu bond length among the $Na_xEu_y(MoO_4)_z$ series, and thus the weakest Eu–Eu interactions.

Although the PLE spectra of the bulk samples were the same and the PL spectra differ only in the intensities of the peaks, the local low loss EELS measurements show a clear difference between the samples with different dimensionalities. This could also be related with the differences in underlying symmetry for the (3 + 1)D (monoclinic) and (3 + 2)D (tetragonal) incommensurately modulated structures.

4. CONCLUSION

The detailed study of phases in the Na_2MoO_4−$Eu_{2/3}MoO_4$ system by TEM has allowed us to differentiate between structures with different modulations that were undetected before by bulk diffraction techniques. Moreover, TEM has also shown clear differences in their low loss EELS spectra. Whereas no satellite reflections were detected on the synchrotron PXRD patterns for $Na_xEu^{3+}{}_{(2-x)/3}\square_{(1-2x)/3}MoO_4$ with $x = 0.286$, a (3 + 2)D incommensurately modulated structure was clearly revealed by TEM. Moreover, TEM showed that for $x = 0.200$, next to the (3 + 1)D incommensurately modulated structure, domains with a (3 + 2)D incommensurately modulated structure are present. For the same $x = 0.286$ and $x = 0.200$ two local minima are observed in the intensity of the Eu^{3+} emission in the spectra of $Na_xEu^{3+}{}_{(2-x)/3}\square_{(1-2x)/3}MoO_4$ ($0.138 \leq x \leq 0.5$) while overall the intensity of the Eu^{3+} emission decreases with decreasing Na^+ content (x) from 0.5 to 0. The maximum luminescence intensity of $Na_5Eu(MoO_4)_4$ (λ_{ex} = 395 nm) in the $^5D_0 \rightarrow {}^7F_2$ transition region is close to the luminescence intensity of YVO_4:Eu^{3+} (λ_{ex} = 326 nm), which makes it suitable as a near-UV converting phosphor to be applied as a red-emitting phosphor for LEDs. For the first time, EELS measurements were performed on these compounds and interesting signatures were found in the low-loss region of the energy spectrum, which are, however, complex and will need further detailed analysis. This method provides insight in the optical spectra on a local scale and confirms the important effect of order in the position and strength of the excitation peaks.

■ AUTHOR INFORMATION

Corresponding Author

*Tel.: +32-32653245. Fax.: +32-32653257. E-mail: j.hadermann@ua.ac.be.

Notes

The authors declare no competing financial interest.

■ ACKNOWLEDGMENTS

This research was supported by FWO (project G039211N), Flanders Research Foundation. V.A.M. and B.I.L. are grateful for financial support of the Russian Foundation for Basic Research (Grants 08-03-00593, 11-03-01164, and 12-03-00124). J.V. and N.G. acknowledge support from the European Research Council under an ERC starting grant No. 278510 VORTEX. J.V. also acknowledges FWO project G.0044.13N.

■ REFERENCES

(1) Shur, M. S.; Zukauskas, A. *Proc. IEEE* **2005**, *93*, 1691.

(2) Yam, F. K.; Hassan, Z. *Microelectron. J.* **2005**, *36*, 129.

(3) Neeraj, S.; Kijima, N.; Cheetham, A. K. *Chem. Phys. Lett.* **2004**, *387*, 2−6.

(4) Kim, T.; Kang, S. *J. Lumin.* **2007**, *122*−*123*, 964−966.

(5) Hwang, K.-S.; Jeon, Y.-S.; Hwangbo, S.; Kim, J.-T. *Opt. Appl.* **2009**, *39* (2), 375−383.

(6) Yan, B.; Wu, J.-H. *Mater. Chem. Phys.* **2009**, *116*, 67−71.

(7) (a) Md. Haque, M.; Lee, H.-I.; Kim, D.-K. *J. Alloys Compd.* **2009**, *481*, 792−796. (b) Zhang, Z. H.; Huang, Q.; Zhao, X.; Zhi Liang Huang, Z. L. *Phys. Status Solidi A* **2009**, *206*, 2839−2843. (c) He, X.; Guan, M.; Li, Z.; Shang, T.; Lian, N.; Zhou, Q. *J. Am. Ceram. Soc.* **2011**, *94*, 2483−2488. (d) Li, Q.; Huang, J.; Chen, D. *Luminescence* **2011**, *26*, 349−355. (e) Khanna, A.; Dutta, P. S. *J. Solid State Chem.* **2013**, *198*, 93−100.

(8) Guo, C.; Gao, F.; Xu, Y.; Liang, L.; Shi, F. G.; Yan, B. *J. Phys. D: Appl. Phys.* **2009**, *42*, 095407.

(9) Li, X. Z.; Lin, Z. B.; Zhang, L. Z.; Wang, G. F. *Mater. Res. Innovations* **2006**, *10*, 50.

(10) Lu, X.; You, Z.; Li, J.; Zhu, Z.; Jia, G.; Wu, B.; Tu, C. *Solid State Commun.* **2008**, *146*, 287−292.

(11) Huang, X.; Wang, G. *J. Phys. D: Appl. Phys.* **2008**, *41*, 22540.

(12) (a) Guo, W.; Chen, Y.; Lin, Y.; Gong, X.; Luo, Z.; Huang, Y. *J. Phys. D: Appl. Phys.* **2008**, *41*, 115409. (b) Chen, Y. J.; Lin, Y. F.; Guo, W. J.; Gong, X. H.; Huang, J. H.; Luo, Z. D.; Huang, Y. D. *Laser Phys. Lett.* **2012**, *9*, 141−144. (c) Zhao, Y.; Huang, Y.; Lin, Z.; Zhang, L.; Wang, G. *Phys. Status Solidi A* **2012**, *209*, 1317−1321.

(13) Shao, Q.; Li, H.; Wu, K.; Dong, Y.; Jiang, J. *J. Lumin.* **2009**, *129*, 879−883.

(14) Yi, L.; Zhou, L.; Wang, Z.; Sun, J.; Gong, F.; Wan, W.; Wang, W. *Curr. Appl. Phys.* **2010**, *10*, 208−213.

(15) Hazen, R. M.; Finger, L. W.; Mariathasan, J. W. E. *J. Phys. Chem. Solids.* **1985**, *46*, 253.

(16) (a) Wang, Z. L.; Liang, H. B.; Wang, J.; Gong, M. L.; Su, Q. *Appl. Phys. Lett.* **2006**, *89*, 071921. (b) Zhao, D.; Cheng, W.-D.; Zhang, H.; Huang, S.-P.; Fang, M.; Zhang, W.-L.; Yang, S.-L. *J. of Molecul. Struct.* **2009**, *919*, 178−184. (c) Zhang, Y.; Xiong, L.; Li, X.; Guo, J.; Wang, Z. *Mater. Sci. Eng. B* **2012**, *177*, 341−344.

(17) Efremov, V. A.; Trunov, V. K.; Berezina, T. *Crystallogr. Rep.* **1982**, *27*, 134−139 (in Russian)..

(18) Efremov, V. A.; Berezina, T.; Averina, I. M.; Trunov, V. K. *Crystallography Reports* **1980**, *25*, 254−261 (in Russian)..

(19) Stedman, N. J.; Cheetham, A. K.; Battle, P. D. *J. Mater. Chem.* **1994**, *4*, 707−711.

(20) Cascales, C.; Méndez Blas, A.; Rico, M.; Volkov, V.; Zaldo, C. *Opt. Mater.* **2005**, *27*, 1672−1680.

(21) Kuz'micheva, G. M.; Lis, D. A.; Subbotin, K. A.; Rybakov, V. B.; Zharikov, E. V. *J. Cryst. Growth* **2005**, *275*, e1835−e1842.

(22) Voron'ko, Y. K.; Subbotin, K. A.; Shukshin, V. E.; Lis, D. A.; Ushakov, S. N.; Popov, A.; Zharikov, E. V. *Opt. Mater.* **2006**, *29*, 246−252.

(23) Méndez-Blas, A.; Rico, M.; Volkov, V.; Zaldo, C.; Cascales, C. *Phys. Rev. B* **2007**, *75*, 174208.

(24) Volkov, V.; Cascales, C.; Kling, A.; Zaldo, C. *Chem. Mater.* **2005**, *17*, 291−300.

(25) Cascales, C.; Serrano, M. D.; Esteban-Betegón, F.; Zaldo, C.; Peters, R.; Petermann, K.; Huber, G.; Ackermann, L.; Rytz, D.; Dupre, C.; Rico, M.; Liu, J.; Griebner, U.; Petrov, V. *Phys. Rev. B* **2006**, *74*, 174114.

(26) Hanuza, J.; Benzar, A.; Haznar, A.; Maczka, M.; Pietraszko, A.; van der Maas, J. H. *Vibrational Spectr.* **1996**, *12*, 25−36.

(27) Rybakova, T. P.; Trunov, V. K. *Zh. Neorg. Khim.* **1974**, *19*, 1631−1636 (in Russian)..

(28) Trunov, V. K.; Evdokimov, A. A.; Rybakova, T. P.; Berezina, T. A. *Zh. Neorg. Khim.* **1979**, *24*, 168−175 (in Russian)..

(29) Morozov, V. A.; Mironov, A. V.; Lazoryak, B. I.; Khaikina, E. G.; Basovich, O. M.; Rossell, M. D.; Van Tendeloo, G. *J. Solid. State Chem.* **2006**, *179*, 1172−1180.

(30) Morozov, V. A.; Arakcheeva, A. V.; Chapuis, G.; Guiblin, N.; Rossell, M. D.; Van Tendeloo, G. *Chem. Mater.* **2006**, *18*, 4075−4082.

(31) Arakcheeva, A.; Pattison, P.; Chapuis, G.; Rossell, M.; Filaretov, A.; Morozov, V.; Van Tendeloo, G. *Acta Cryst., Sect. B* **2008**, *64*, 160−171.

(32) Morozov, V.; Arakcheeva, A.; Redkin, B.; Sinitsyn, V.; Khasanov, S.; Kudrenko, E.; Raskina, M.; Lebedev, O.; Van Tendeloo, G. *Inorg. Chem.* **2012**, *51*, 5313−5324.

(33) Arakcheeva, A.; Chapuis, G. *Acta Cryst., Sect. B* **2008**, *64*, 12−25.

(34) Arakcheeva, A.; Logvinovich, D.; Chapuis, G.; Morozov, V.; Eliseeva, S. V.; Bünzli, J.-C. G.; Pattison, P. *Chem. Sci.* **2012**, *3*, 384−390.

(35) Van Smaalen, S.; Campbell, B. J.; Stokes, H. T. *Acta Crystallogr., Sect. A* **2013**, *69*, 75.

(36) Stevens, S. B.; Morrison, C. A.; Allik, T. H.; Rheingold, A. L.; Haggerty, B. S. *Phys. Rev. B* **1991**, *43*, 7386−7394.

(37) Blasse, G.; Bril, A.; Nieuwpoort, W. C. *J. Phys. Chem. Solids* **1966**, *27*, 1587−1592.
(38) Shannon, R. D. *Acta Crystallogr., Sect. A* **1976**, *32*, 751.
(39) Xie, A.; Ximing Yuana, X.; Wanga, F.; Shi, Y.; Li, J.; Liua, L.; Mu, Z. *J. Alloys Compd.* **2010**, *501*, 124−129.
(40) Zhao, C.; Yin, X.; Huang, F.; Hang, Y. *J. Solid. State Chem.* **2011**, *184*, 3190−3194.
(41) Chiu, C.-H.; Liu, C.-H.; Huang, S.-B.; Chen, T.-M. *J. Electrochem. Soc.* **2008**, *155*, J71−J78.
(42) (a) Palilla, F. C.; Levine, A. K. *Appl. Opt.* **1966**, *5*, 1467−1468. (b) Huignard, A.; Gacoin, T.; Boilot, J. P. *Chem. Mater.* **2000**, *12*, 1090−1094. (c) Li, G.; Chao, K.; Peng, H.; Chen, K. *J. Phys. Chem., Sect. C* **2008**, *112*, 6228−6231. (d) Xu, Z.; Kang, X.; Li, C.; Hou, Z.; Zhang, C.; Yang, D.; Li, G.; Lin, J. *Inorg. Chem.* **2010**, *49*, 6706−6715. (e) Li, Y.; Zheng, Y.; Wang, Q.; Zhang, C. C. *Mater. Chem. Phys.* **2012**, *135*, 451−456.